Figures 1 and 2. This work was supported by grant GM43238 from the National Institutes of Health.

Biographical Sketch

H. Jane Dyson. *b* 1951. B.Sc.(hons), 1973; Ph.D. 1977, Sydney. Postdoctoral in Biology, MIT, 1977–78, Chemistry faculty, University of New South Wales, 1979–1984. NMR work begun in earnest at Scripps Clinic in 1984 in collaboration with Peter Wright; faculty at Scripps 1984–present. Approx. 50 publications. Research interests in the conformation of short peptides and in structure–function studies of proteins including thioredoxin.

Three-Dimensional HMQC–NOESY, NOESY–HMQC, & NOESY–HSQC

Ranjith Muhandiram & Lewis E. Kay
University of Toronto, Toronto, ON, Canada

1 INTRODUCTION

The widespread application of NMR in the study of macromolecular structure is to a large extent the result of the ^1H–^1H nuclear Overhauser effect (NOE), whereby it is possible to obtain distance information relating spatially proximate protons (see ***Nuclear Overhauser Effect***). For reasonably small molecules (for example, proteins consisting of ~100 or fewer residues) this information is readily available from two dimensional (2D) homonuclear NOESY spectra which consist of cross peaks, with intensities related to the distance between the participating spins[1] (see also ***NOESY*** and ***Biological Macromolecules: Structure Determination in Solution***). Because NOE peaks between a particular proton and all other protons within a radius of approximately 0.5 nm can, in principle be observed, the number of potential NOE cross peaks increases rapidly with molecular weight. This gives rise to considerable overlap in 2D NOE spectra of large molecules (>10 kDa), making it difficult to assign cross peaks and to obtain accurate distance information. An elegant approach to removing cross-peak overlap in 2D NOE spectra is to resolve the 2D spectrum along a third frequency dimension, the ^{15}N or ^{13}C chemical shift of the heteronucleus directly attached to one of the protons participating in the NOE transfer[2,3] (see also ***Three- & Four-Dimensional Heteronuclear Magnetic Resonance***). Such three-dimensional heteronuclear chemical shift correlated-NOESY spectra contain the same numbers of cross peaks as in a regular 2D NOESY spectrum, but the information content of these spectra (i.e., the cross peaks) is dispersed over the chemical shift range of the heteronucleus. Because of the low natural abundance of ^{15}N and ^{13}C, isotopic enrichment is necessary in order to obtain spectra with high sensitivity.[2,4]

Figure 1 illustrates the resolving power of ^{15}N-edited 3D heteronuclear NOE spectroscopy. In (a), a region from the regular 2D NOESY spectrum of the protein staphylococcal nuclease (18 kDa) is illustrated. In (b), the corresponding region is shown illustrating NOEs to NH protons attached to ^{15}N nuclei resonating at 122.3 ppm. The simplification is clearly evident.

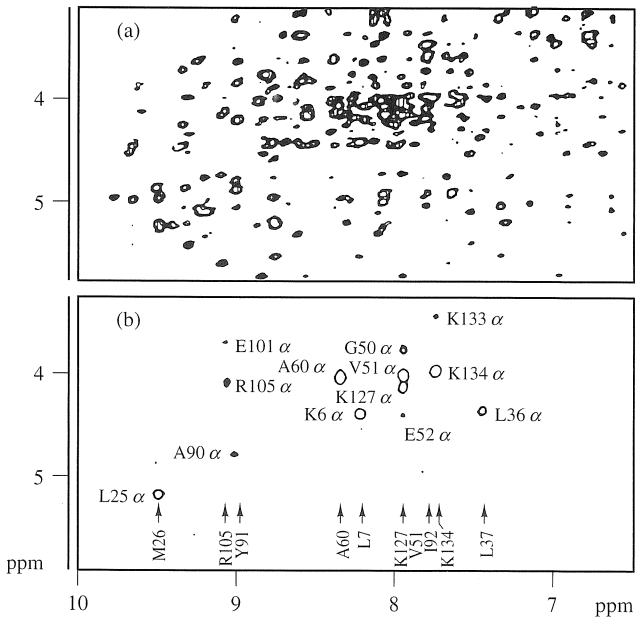

Figure 1 Comparison of NH, $C_\alpha H$ cross peak regions from 2D NOESY and 3D NOESY–HMQC experiments recorded at 500 MHz on a 1.5 mM sample of ^{15}N-labeled staphylococcal nuclease in 90% H_2O using a 125 ms NOE mixing time. (a) Regular 2D NOESY spectrum; (b) Corresponding region in a slice from the 3D NMR spectrum, where (^1H,NH) cross peaks are separated according to the ^{15}N chemical shift of the amide nitrogen one-bond-coupled to the NH proton. The section displays NH, $C_\alpha H$ correlations only for those amides that have an ^{15}N chemical shift of 122.3 ± 0.3 ppm. The 3D data set was collected as a 128 × 32 × 256 complex matrix (t_1, t_2, t_3). Sixteen transients were accumulated for each FID, and the total experimental time was about 64 h. Data were zero filled prior to Fourier transformation to yield a 256 × 64 × 512 data matrix (F_1, F_2, F_3) for the absorptive part of the spectrum. (Source: A. Bax, *Annu. Rev. Biochem.*, 1989, **58**, 223)

The simplification of a crowded NOESY spectrum as a result of the resolving power of the heteronuclear chemical shift enables the unambiguous assignment of many of the cross peaks, facilitates the use of automated peak picking and assignment methods, and significantly increases the effective molecular weight limitations of NMR. The method has been used for the structure elucidation of proteins having molecular weights as large as ~25 kDa,[5,6] RNA,[7] and oligosacharides.[8] In the following sections, descriptions of many of the pulse sequences currently in use are given, with emphasis on the 3D NOESY–HMQC sequence and improved versions of NOESY–HSQC with pulsed field gradients. In addition, protein applications of these experiments are highlighted.

2 HMQC(HSQC)–NOESY AND NOESY–HMQC (HSQC) EXPERIMENTS

The heteronuclear correlated 3D NOESY experiment consists of elements of (i) the regular 2D ^{1}H–^{1}H NOESY experiment and (ii) the proton-detected heteronuclear chemical shift correlation experiment. The latter element can be of the HMQC (heteronuclear multiple quantum correlation)[9] or HSQC (heteronuclear single quantum correlation)[10] variety, giving rise to 3D NOESY–HMQC, 3D HMQC–NOESY or 3D NOESY–HSQC, 3D HSQC–NOESY experiments, respectively. In these heteronuclear three-dimensional experiments, the flow of magnetization is controlled by the editing effect of the heteronucleus. In what follows, a brief discussion of the HMQC–NOESY[11] experiment will be provided, followed by a more detailed examination of the NOESY–HMQC[12] scheme. In subsequent sections, some HSQC versions of the experiments will be described.

2.1 3D HMQC–NOESY

Figure 2(a) illustrates one version of the HMQC–NOESY pulse scheme.[11] In order to ensure maximum sensitivity, magnetization originates on the sensitive proton spin, and proton magnetization is also detected during acquisition (t_3). Proton magnetization is recorded during t_1, with the effects of the large one-bond ^{1}H–X scalar coupling refocused through the action of the 180° X pulse applied in the middle of the t_1 evolution period. Subsequently, antiphase magnetization is generated during the τ ($\leqslant [2J_{HX}]^{-1}$) delay and converted into ^{1}H–X double and zero quantum coherence by the application of the first 90° X pulse. The chemical shift of the heteronucleus is recorded during the t_2 delay. The ^{1}H 180° pulse applied in the center of the t_2 evolution delay interconverts zero and double quantum coherences, so that effectively only X chemical shift is allowed to evolve during this period. Subsequently, antiphase proton magnetization is regenerated with the application of the second 90° X pulse, and refocusing due to the ^{1}H–X scalar coupling is allowed to occur during the second τ delay. Because of the phase cycle on the first 90° X pulse, only magnetization originating from proton spins directly coupled to X spins is retained. During the mixing time, magnetization on X-nucleus attached proton spins is transferred to all protons in close proximity. Therefore, during the acquisition time t_3, protons that resonate in the entire proton chemical shift range may be detected. Thus, for an ^{15}N-labeled protein (X = ^{15}N) dissolved in H_2O, the acquisition dimension is similar to the acquisition dimension of a regular 2D NOESY experiment. The final 3D spectrum consists of a set of 2D ^{1}H–^{1}H (F_1/F_3) NOESY maps separated according to the amide ^{15}N chemical shift along the third frequency dimension (F_2). In contrast to the indirectly detected dimension of a regular 2D NOESY map, the F_1 dimension of each F_1/F_3 plane consists of signals originating only from protons attached to ^{15}N, owing to the editing effect of the HMQC part of the sequence. Despite the spectral simplification attainable with ^{15}N chemical shift separation in the third dimension, protein NH, C_αH cross peaks can

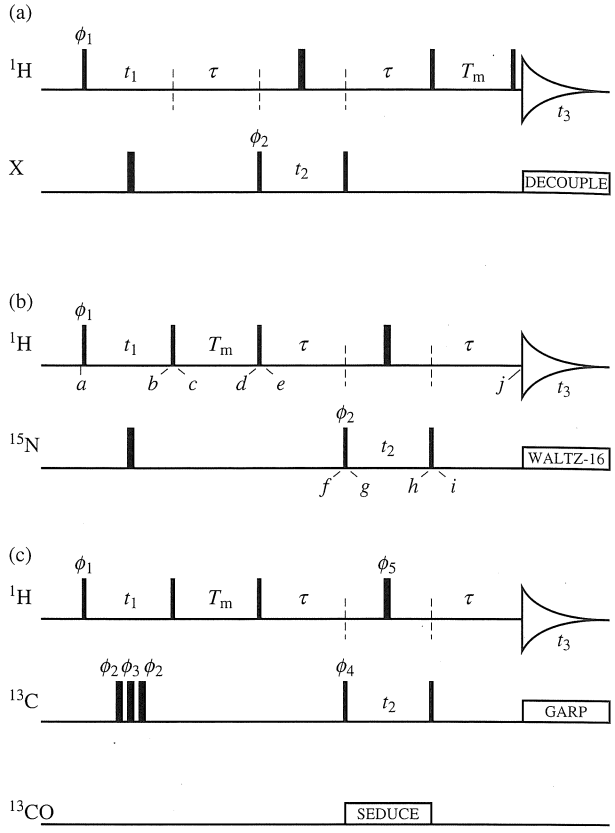

Figure 2 Pulse sequences for (a) 3D HMQC–NOESY, and (b), (c) 3D NOESY–HMQC experiments. Narrow (wide) pulses are applied with a flip angle of 90° (180°). Unless otherwise indicated all pulses are applied along the x axis. All ^{1}H and ^{13}C pulses are applied at the highest field possible (about 20 kHz), while typical ^{15}N pulses are applied with a field of about 5–6 kHz. The delay τ is set to slightly less than $[2J(X,H)]^{-1}$ to minimize relaxation losses. Quadrature in t_1 and t_2 is achieved via States–TPPI[13] of ϕ_1 and ϕ_2, respectively [sequences (a) and (b)], and ϕ_1 and ϕ_4, respectively [sequence (c)]. In (b), τ = 4.5 ms, and ^{15}N decoupling is achieved with a 1 kHz WALTZ-16[14] decoupling field. In (c), τ = 3.3 ms. During t_3, ^{13}C decoupling is achieved with a GARP[15] sequence using a 3.5–4.0 kHz field, and ^{13}CO decoupling during t_2 is achieved with a SEDUCE-1[16] field (about 1.5 kHz at peak height) centered at 175 ppm. The ^{13}C 180° pulse in the center of t_1 is of the composite variety. The phase cycling employed in (a) is ϕ_1 = 2(x),2($-x$); ϕ_2 = x,$-x$; Rec. = x,2($-x$),x; the phase of the last ^{1}H pulse is incremented by 90° with the receiver phase after every four transients. That in (b) is ϕ_1 = x,$-x$; ϕ_2 = 2(x),2($-x$); Rec. = x,2($-x$),x. That in (c) is ϕ_1 = x,$-x$; ϕ_2 = 2(x),2($-x$); ϕ_3 = 2(y),2($-y$); ϕ_4 = 8(x),8($-x$); ϕ_5 = 4(x),4($-x$); Rec. = 4(x,$-x$),4($-x$,x). [Adapted from (a) Fesik and Zuiderweg;[11] (b) Marion et al.,[12] and (c) Ikura et al.[17]]

be obscured if the $C_\alpha H$ resonates close to the water resonance. Therefore, applications of this experiment have primarily been for samples dissolved in D_2O with X = ^{13}C, and the reverse version, the NOESY–HMQC experiment, where the crucial NH, $C_\alpha H$ cross peaks are easily observed, has been the preferred choice for ^{15}N-labeled protein samples dissolved in H_2O.

2.2 3D ^{15}N-Edited NOESY–HMQC

Figure 2(b) illustrates the pulse scheme used to record 3D ^{15}N-edited NOESY–HMQC spectra of ^{15}N-labeled molecules.[12] The flow of magnetization during the course of the pulse sequence is conveniently described using the product operator formalism.[18] A simplified description of the magnetization transfer events is presented here. Let $\hat{I}_a$ and $\hat{I}_b$ be spin operators for two protons in close proximity, with only spin b coupled to an ^{15}N spin, denoted by the operator $\hat{N}$. The effects of relaxation during all delays, with the exception of the mixing time, are neglected. At point a in the pulse scheme of Figure 2(b), the equilibrium density operator is given by $\hat{I}_{az}$ and $\hat{I}_{bz}$ for spins a and b respectively. The behavior of magnetization from point a to the beginning of the mixing period T_m (point c) is described by

$$\begin{array}{llll} \hat{I}_{az} & \{a\} \xrightarrow{90°\mathrm{H}} & -\hat{I}_{ay} \xrightarrow{t_1} & -\hat{I}_{ay}\cos(\omega_a t_1) + \hat{I}_{ax}\sin(\omega_a t_1) \quad \{b\} \\ \hat{I}_{bz} & \{a\} & -\hat{I}_{by} & -\hat{I}_{by}\cos(\omega_b t_1) + \hat{I}_{bx}\sin(\omega_b t_1) \quad \{b\} \end{array} \tag{1}$$

$$\begin{array}{ll} \xrightarrow{90°\mathrm{H}} & -\hat{I}_{az}\cos(\omega_a t_1) \quad \{c\} \\ & -\hat{I}_{bz}\cos(\omega_b t_1) \quad \{c\} \end{array}$$

where the letters in curly brackets { } denote the positions in the sequence where the appropriate density operators apply and ω_i is the resonance frequency of spin i (a,b). Note that the effects of ^1H–^{15}N scalar coupling are refocused by the end of the t_1 period due to the application of the ^{15}N 180° pulse in the center of this delay. Depending on the relative phases of the first two ^1H 90° pulses, either the cosine- or the sine-modulated component of magnetization is stored along the z axis at point c. One approach to obtaining quadrature in F_1 is to store both components in separate memory locations and subsequently combine them by the method of States et al.[19] In what follows, only the first line of the phase cycle that appears in the legend to Figure 2(b) is assumed (i.e., $\phi_1 = \phi_2 = x$). In the case of macromolecular applications, the transverse components of magnetization [e.g., $\hat{I}_{ax}\sin(\omega_a t_1)$ and $\hat{I}_{bx}\sin(\omega_b t_1)$] that are present at the beginning of the mixing period decay rapidly as a result of short transverse relaxation times, and have therefore been omitted from equation (1). The use of a pulsed field gradient during this delay and/or the appropriate phase cycling can eliminate signals arising from such terms.

During the mixing period T_m, magnetization is transferred between proximate protons:

$$\begin{array}{llll} -\hat{I}_{az}\cos(\omega_a t_1) & \{c\} \xrightarrow{T_m} & -A\hat{I}_{az}\cos(\omega_a t_1) - A'\hat{I}_{bz}\cos(\omega_a t_1) & \{d\} \\ -\hat{I}_{bz}\cos(\omega_b t_1) & \{c\} & -B\hat{I}_{bz}\cos(\omega_b t_1) - B'\hat{I}_{az}\cos(\omega_b t_1) & \{d\} \end{array} \tag{2}$$

where A, A', B, and B' are constants that depend on the mixing time, the inverse sixth power of the distance between spins a and b and the motional properties of the internuclear vector connecting spins a and b. The values of A, A', B, and B' are easily obtained by solving the set of coupled differential equations that describe cross relaxation between spins a and b. Details can be found in the text by Noggle and Schirmer,[20] and will not be repeated here. In general, $A' = B'$. Since only proton b is attached to a nitrogen spin N, the only terms of the density operator that give rise to observable magnetization after the HMQC portion of the sequence (with the appropriate phase cycling of ϕ_2) are those proportional to $\hat{I}_{bz}$. Following the conversion into transverse proton magnetization by the proton 90° pulse at point d in the sequence, these terms evolve into proton magnetization that is antiphase with respect to spin N during the first τ period:

$$\begin{array}{llll} -A'\hat{I}_{bz}\cos(\omega_a t_1) & \{d\} \xrightarrow{90°\mathrm{H}} & A'\hat{I}_{by}\cos(\omega_a t_1) & \{e\} \\ -B\hat{I}_{bz}\cos(\omega_b t_1) & \{d\} & B\hat{I}_{by}\cos(\omega_b t_1) & \{e\} \end{array} \tag{3}$$

$$\begin{array}{ll} \xrightarrow{\tau} & -A'2\hat{I}_{bx}\hat{N}_z\cos(\omega_a t_1) \quad \{f\} \\ & -B2\hat{I}_{bx}\hat{N}_z\cos(\omega_b t_1) \quad \{f\} \end{array}$$

In the derivation of equation (3) the delay τ has been set equal to $[2J(\mathrm{N,H})]^{-1}$. In addition, ^1H chemical shift evolution during τ has been neglected, since the ^1H 180° pulse applied in the center of the t_2 evolution period refocuses the effect of proton chemical shifts. The 90° ^{15}N pulse at point f creates zero and double quantum terms, which subsequently evolve in t_2 to give N-spin chemical shift labeling:

$$\begin{array}{llll} -A'2\hat{I}_{bx}\hat{N}_z\cos(\omega_a t_1) & \{f\} \xrightarrow{90°\mathrm{N}} & A'2\hat{I}_{bx}\hat{N}_y\cos(\omega_a t_1) & \{g\} \\ -B2\hat{I}_{bx}\hat{N}_z\cos(\omega_b t_1) & \{f\} & B2\hat{I}_{bx}\hat{N}_y\cos(\omega_b t_1) & \{g\} \end{array} \tag{4}$$

$$\begin{array}{ll} \xrightarrow{\frac{1}{2}t_2\ 180°\mathrm{H}\ \frac{1}{2}t_2} & A'2\hat{I}_{bx}\hat{N}_y\cos(\omega_a t_1)\cos(\omega_N t_2) \quad \{h\} \\ & B2\hat{I}_{bx}\hat{N}_y\cos(\omega_b t_1)\cos(\omega_N t_2) \quad \{h\} \end{array}$$

where the $\sin(\omega_N t_2)$ terms have been neglected, since for $\phi_2 = x$ these terms do not contribute to the observed signal.

After the second 90° N pulse, the double and zero quantum terms are converted into antiphase proton magnetization, which is allowed to refocus into observable proton magnetization during the second τ delay. Evolution during the acquisition time t_3 then yields

$$\begin{array}{ll} A'\hat{I}_{by}\cos(\omega_a t_1)\cos(\omega_N t_2) & \{j\} \\ B\hat{I}_{by}\cos(\omega_b t_1)\cos(\omega_N t_2) & \{j\} \end{array} \tag{5}$$

$$\begin{array}{ll} \xrightarrow{t_3} & A'\hat{I}_{by}\cos(\omega_a t_1)\cos(\omega_N t_2)\cos(\omega_b t_3) \ \text{(cross peak)} \\ & B\hat{I}_{by}\cos(\omega_b t_1)\cos(\omega_N t_2)\cos(\omega_b t_3) \ \text{(diagonal peak)} \end{array}$$

for the y component of magnetization. Similar relations hold for the x component of magnetization.

Fourier transformation of the resultant signal gives rise to cross peaks at (ω_a,ω_b) located in a slice through the 3D data set with ^{15}N frequency ω_N. In addition, a diagonal peak at (ω_b,ω_b) in the same slice is also observed. That is, a NOE cross peak at the chemical shift of the proton from which magnetization originated (F_1), the chemical shift of the destination NH proton (F_3), and the shift of the ^{15}N nucleus directly coupled to the NH spin (F_2) are obtained. Unlike 2D ^1H–^1H NOESY

For References see p. 4743

maps, which are symmetrical, ^{15}N-edited maps are asymmetrical, since the ^{15}N editing that occurs during the course of the pulse scheme ensures that only the transfer of magnetization to an NH proton is observed. Note that the crucial (C_αH, NH) NOE connectivities occur as (F_1,F_3) cross peaks, and can be detected in a straightforward manner without interference from the residual water signal, as shown in Figure 1.

2.2.1 *Practical Aspects of 3D Heteronuclear-Edited NOESY Pulse Schemes*

2.2.1.1 Water Suppression. Because ^{15}N-edited NOESY experiments provide crucial information linking NH protons to neighboring proton spins, these experiments must be performed on protein samples dissolved in H_2O. Water suppression schemes must therefore be employed to minimize the dynamic range problem that the use of this solvent presents. Suppression of the intense water signal is often achieved through the use of a weak coherent presaturation field ($\leqslant$30 Hz) applied during the relaxation delay prior to the first 90° excitation pulse. In addition, saturation of the water resonance can proceed during the mixing time. In an early implementation of the experiment, Kay et al.[21] described the use of an off-resonance DANTE[22] sequence to suppress the water, with the carrier positioned in the center of the NH region. In addition, an off-resonance jump and return sequence of the type, $45°_x$–τ–$45°_x$, where τ is set according to the relation $\tau = (2 \times \text{offset of } H_2O)^{-1}$ and where the carrier is centered in the NH region, was inserted in place of the 90° ^{1}H pulse applied immediately after the mixing period.

The use of presaturation has been shown significantly to decrease the intensity of cross peaks originating from labile protons. This can lead to a significant overall decrease in the intensity of the protein envelope due to the effect of saturation transfer. We have recently shown in applications involving the cellulose binding domain of a cellulase from *Cellulomonas fimi* (CBD, a dimer of monomers of molecular weight 11 kDa) that the use of a presaturation field (30 Hz) applied for 1 s prior to the start of the experiment can decrease the protein envelope by as much as 40%.[23] Montelione and co-workers have recently compared a number of different water suppression schemes as a function of sample pH, showing that presaturation gives the largest decrease in signal.[24] Grzesiek and Bax have also emphasized the importance of not saturating the water resonance,[25] and have suggested a strategy involving the use of pulsed field gradients and selective pulses on the water to ensure the placement of water magnetization on the $+z$ axis prior to the start of the detection period in each transient. Pulse schemes incorporating field gradients are discussed in Section 3.

2.2.1.2 Phasing in the indirectly detected dimensions (F_1, F_2). After Fourier transformation, the indirectly detected dimensions can be phased using calculated phase parameters. The approach of choice is to set the initial values of t_1 and t_2 [$t_1(0)$, $t_2(0)$] prior to running the experiment in order to obtain spectra having first-order phase corrections of either 0° or 180°. This ensures that flat baselines are obtained.[26] It is straightforward to calculate the appropriate values for $t_1(0)$ and $t_2(0)$ for a given pulse sequence, and in what follows we consider the ^{15}N NOESY–HMQC sequence of Figure 2(b). Noting that, to a good first approximation, a 90° pulse can be replaced by a delta function pulse followed by a delay of $(2/\pi)\tau_{90}$, where τ_{90} is the 90° pulse width,[27] the sampling delay in the t_1 dimension (NOESY portion of the sequence) is given by

$$sd(t_1) = \frac{4}{\pi}\tau_{90}(\mathrm{H}) + \tau_{180}(\mathrm{N}) + t_1(0) \qquad (6)$$

where τ_{90}(H) is the ^{1}H 90° pulse width and τ_{180}(N) is the ^{15}N 180° pulse width. The sampling delay in the t_2 dimension (the HMQC portion of the sequence) is given by

$$sd(t_2) = \frac{4}{\pi}\tau_{90}(\mathrm{N}) + \tau_{180}(\mathrm{H}) + t_2(0) \qquad (7)$$

where τ_{180}(H) is the duration of the ^{1}H 180° pulse in the middle of t_2.[21]

If the data are acquired in the States format, the linear phase correction that must be applied in F_i (i = 1, 2) is given by $sd(t_i) \times 360/\Delta t_i$, where Δt_i is the dwell time in the t_ith dimension.[26] In order to ensure that no net phase correction is applied in the center of the spectrum, a zeroth-order phase correction of $-0.5sd(t_i) \times 360/\Delta t_i$ must be applied as well. It should be clear that if the sampling is delayed by exactly $\frac{1}{2}\Delta t_i$, a linear phase correction of 180° is required across the spectrum. In this case, aliased peaks will be of opposite sign relative to peaks that are not aliased.

2.3 Application to Uniformly ^{13}C-Enriched Molecules

The ^{13}C NOESY–HMQC and HMQC–NOESY experiments provide valuable distance information linking two carbon-bound protons. For reasons of sensitivity, these experiments, like the ^{15}N versions discussed previously, are performed on highly enriched, uniformly labeled samples. The use of highly enriched ^{13}C molecules results in a significant increase in the linewidths of the attached proton(s). The heteronuclear dipolar coupling between a directly coupled ^{13}C–^{1}H pair is approximately a factor of two larger than the coupling from an ^{15}N–^{1}H spin pair. A second complication associated with the use of uniform labeling is the introduction of homonuclear carbon–carbon scalar couplings, varying from approximately 60 Hz for $^{13}C_\alpha$–^{13}CO couplings to approximately 35 Hz for aliphatic carbons. These couplings can significantly degrade the resolution available in spectra. Fortunately, the large chemical shift difference between carbonyl spins and the aliphatic spins allows for the efficient decoupling of the $^{13}C_\alpha$–^{13}CO scalar interaction using selective shaped decoupling schemes such as SEDUCE-1.[16] In order to minimize the effects of the aliphatic couplings, maximum acquisition times $t_{max} \approx 10$ ms are chosen in the carbon dimension, where $t_{max} < [2J(\mathrm{C,C})]^{-1}$ and J(C,C) is the aliphatic scalar coupling constant. While this does limit resolution in the carbon dimension, it must be kept in mind that in many protein applications, the ^{13}C T_2 values are on the order of only 10–20 ms.

Figure 2(c) illustrates a pulse scheme for the ^{13}C NOESY–HMQC sequence.[17] The flow of magnetization is essentially identical to that discussed in connection with the ^{15}N-edited version of the experiment, and will therefore only be summarized as follows:

$$^1\mathrm{H}_i(t_1) \xrightarrow{\mathrm{NOE}} {}^1\mathrm{H}_j \xrightarrow{J(\mathrm{C,H})} {}^{13}\mathrm{C}_j(t_2) \xrightarrow{J(\mathrm{C,H})} {}^1\mathrm{H}_j(t_3) \qquad (8)$$

with chemical shift evolution recorded during t_1, t_2, and t_3. Note that the reverse pathway, where magnetization originates

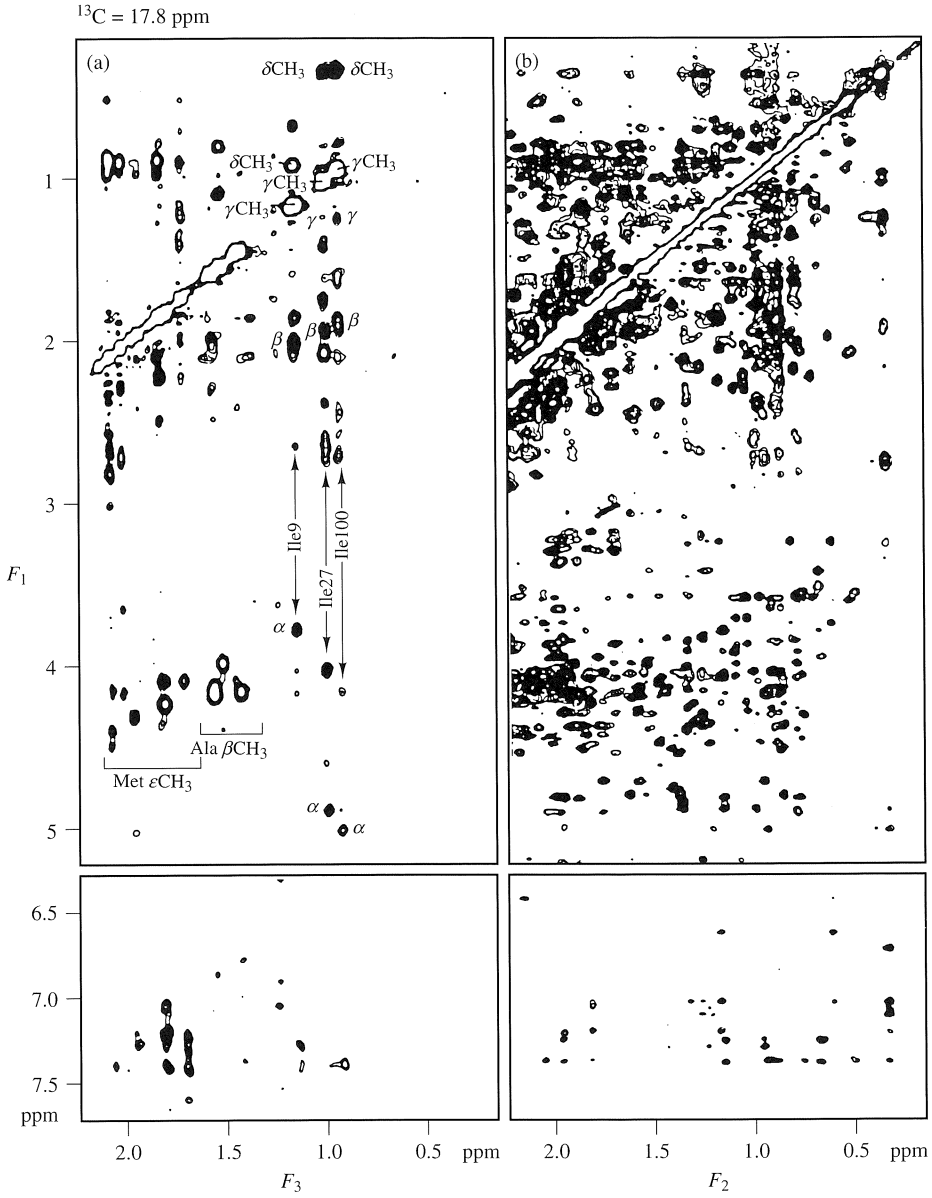

Figure 3 Comparison of (a) a section of an (F_1, F_3) slice taken at F_2 = 17.8 ppm from the 500 MHz 3D ^{13}C NOESY–HMQC spectrum of a 1.5 mM 95% ^{13}C-labeled sample of calmodulin, 6.2 mM Ca^{2+} and (b) the same region of the 600 MHz regular 2D NOESY spectrum of a 1.5 mM unlabeled calmodulin sample, 6.2 mM Ca^{2+}, using mixing times of 120 ms. The 3D data set was collected as a matrix of 128* × 64* × 512 points (t_1, t_2, t_3) in about 60 h (* denotes complex points). (Reproduced by permission of Academic Press from M. Ikura, L. E. Kay, R. Tschudin, and A. Bax, *J. Magn. Reson.*, 1990, **86**, 204)

on spin j and is transferred via the NOE to spin i, is also possible (providing that both proton spins i and j are bound to ^{13}C nuclei), so that symmetry related cross peaks are observed at (H_i,C_j,H_j) and (H_j,C_i,H_i). For the case of distinct carbons C_i and C_j, the symmetry related cross peaks will appear on different slices in the 3D data set. These symmetry related pairs are extremely helpful in the unambiguous assignment of NOE cross peaks.

Because of the large carbon chemical shift range, extending from approximately 10 ppm for methyl carbons to 140 ppm for aromatic carbons, many of the cross peaks in the 3D ^{13}C-edited NOESY spectra are aliased in the carbon dimension. Typically, a carbon spectral width of 3–4 kHz is employed with the carbon carrier positioned at about 65 ppm. The sampling delay in the carbon dimension is adjusted so that a 180° first-order phase correction is required. In this way, cross peaks that have been aliased an odd number of times are 180° out of phase relative to peaks that are not aliased or have been aliased an even number of times.

Figure 3 illustrates the power of the 3D ^{13}C NOESY–HMQC experiment in removing the overlap in the crowded aliphatic region of the regular NOESY spectrum. A comparison of a slice from the 3D data set recorded on the protein calmodulin (MW = 16.7 kDa) with the same region of a 2D spectrum clearly shows the resolving power in increasing the dimensionality from two to three.[17]

For References see p. 4743

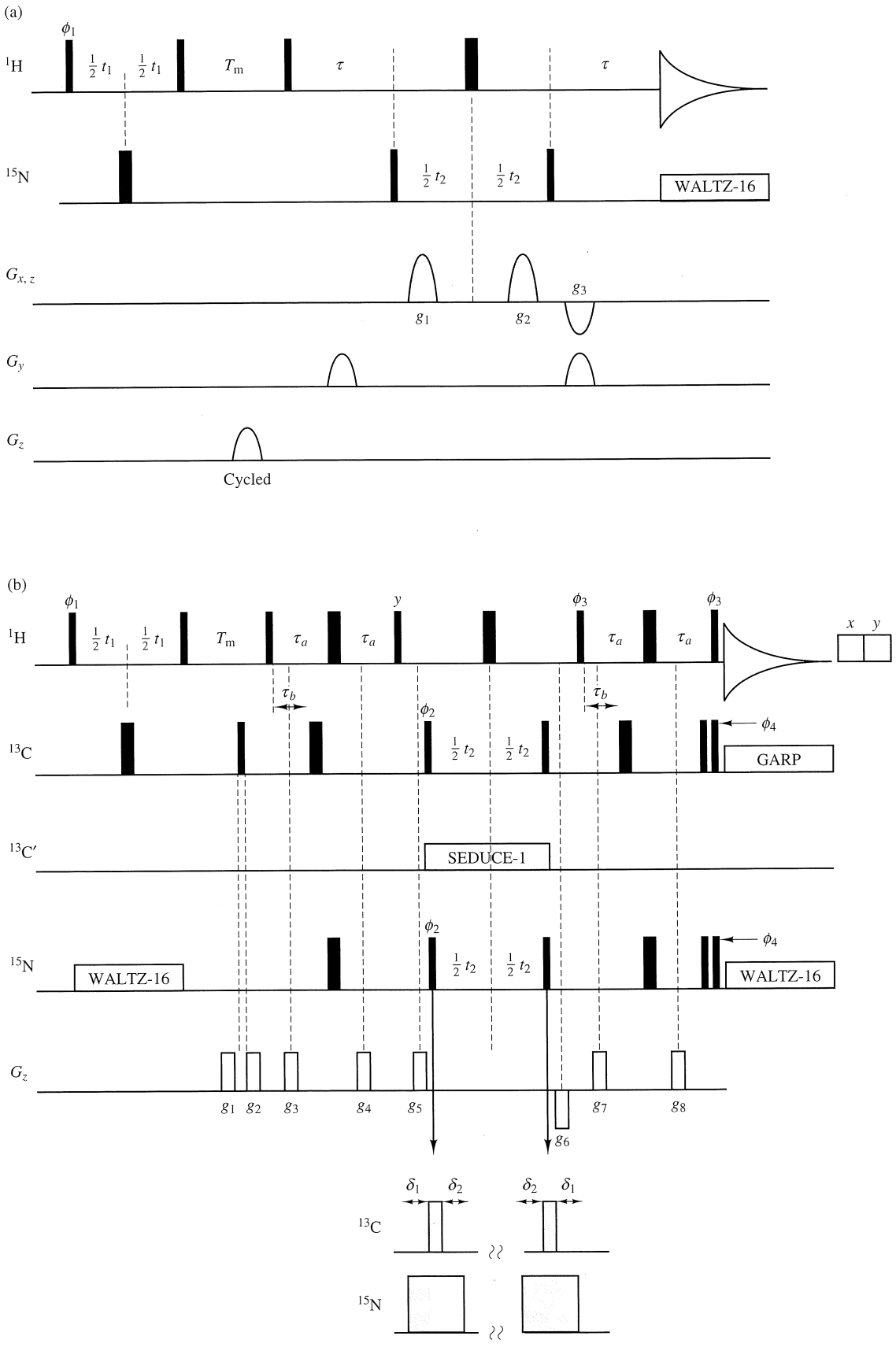

Figure 4

For list of General Abbreviations see end-papers

Up to this point in our discussion, we have focused on a number of the basic NOESY–HMQC and HMQC–NOESY pulse sequences, as they appeared in the literature, prior to the development of pulsed field gradient methods. It is generally the case that these experiments can be significantly improved with the incorporation of field gradients, and the use of this novel technology in such applications is discussed in the next section.

3 PULSED FIELD GRADIENT METHODS

Recent developments in pulsed field gradient technology have led to many useful applications in high-resolution NMR spectroscopy (see ***Field Gradients & Their Application***). The use of gradients allows for the efficient removal of the intense water signal in the case of samples dissolved in H_2O,[28] the elimination of undesired coherences that produce artifacts,[29] a decrease in the number of phase cycling steps, thereby reducing the overall data collection time for sufficiently concentrated samples,[30] and the selection of particular coherence transfer pathways.[31] By incorporating field gradient pulses into many of the experiments discussed earlier, data sets with improved suppression of solvent and artifacts can be obtained. A brief discussion of two heteronuclear-edited gradient NOESY experiments is presented; an ^{15}N-edited NOESY–HMQC experiment developed by Vuister et al.[30] that can be recorded using only a single transient for each ^{15}N data point, and a simultaneous ^{15}N-, ^{13}C-edited NOESY–HSQC experiment.[32]

3.1 Gradient 3D NOESY–HMQC

A pulse scheme for the gradient-enhanced 3D NOESY–HMQC experiment developed by Vuister and co-workers is shown in Figure 4(a).[30] In this experiment, the coherence transfer pathway whereby magnetization passes through nitrogen is selected with the use of the appropriate pulsed field gradients. Because it is not possible for water magnetization to traverse this pathway, excellent levels of water suppression can be achieved. The gradients g_1–g_3 are employed for coherence transfer selection by adjusting their strengths according to the ratio $g_1:g_2:g_3 = 4.94:4.94:1.0$ ($\gamma_H/\gamma_N = -9.88$), while the gradient pair (G_y) applied on opposite sides of the ^{1}H 180° pulse in the middle of the t_2 period ensures that any artifacts that could be created owing to imperfections in this pulse are eliminated.[29] In this experiment, pure amplitude-modulated data are recorded in the t_1 dimension in the normal fashion. However, the use of gradients g_1–g_3 results in the generation of phase-modulated data in the t_2 dimension, and therefore spectra must be presented in the absolute value mode after processing. Note that phase cycling is not necessary in the present application. Thus, it is possible to obtain spectra in short periods of measuring time, assuming that the sample is sufficiently concentrated so that the signal-to-noise ratio is not limiting. For this reason, this experiment is useful for kinetic studies and for studies of molecules that are stable for only short periods of time. The requisite absolute value representation of the data, however, does result in a considerable loss in resolution, which is especially critical in macromolecular applications.

3.2 Simultaneous ^{15}N-,^{13}C-Edited NOESY

An advantage associated with the development of pulsed field gradient technology is the potential of recording all spectra necessary for a protein structure determination using only a single ^{15}N-,^{13}C-labeled sample dissolved in H_2O. In addition to minimizing the number of samples necessary for a structure determination, the use of just a single sample also ensures that ambiguities arising from a comparison of data recorded on a number of different samples prepared with slight differences can be minimized. This is important in order to maximize the efficiency of automated or semi-automated assignment and structure determination approaches.

The CN NOESY–HSQC experiment illustrated in Figure 4(b) provides NOEs between any two proximate protons in ^{15}N-,^{13}C-labeled proteins separated by the chemical shift of the heteroatom to which the destination proton is attached.[32] Because spectra are recorded on samples dissolved in H_2O, valuable NOEs involving NH protons are also observed.

Pulsed field gradients are used in this experiment to aid in the removal of artifacts as well as to assist in water suppres-

Figure 4 Pulse sequences for (a) the gradient NOESY–HMQC and (b) the gradient CN NOESY–HSQC experiments. Narrow (wide) pulses are applied with a flip angle of 90° (180°). Unless otherwise indicated, all pulses are applied along the x axis. All ^{1}H and ^{13}C pulses are applied at the highest field possible (about 20 kHz), while typical ^{15}N pulses are applied with a field of about 5–6 kHz. In (a), quadrature in t_1 is achieved via States–TPPI[13] of ϕ_1; $\tau = 4.5$ ms. Gradients are of 0.8 ms in duration and are sine-bell in shape. Gradient strengths are $g_{1x} = g_{2x} = 63.7\,\mathrm{mT\,m^{-1}}$, $g_{3x} = -12.9\,\mathrm{mT\,m^{-1}}$, $g_{1z} = g_{2z} = 20.5\,\mathrm{mT\,m^{-1}}$, $g_{3z} = -4.2\,\mathrm{mT\,m^{-1}}$, and $G_y = 19.7\,\mathrm{mT\,m^{-1}}$. The G_z gradient in T_m is applied for 0.4 ms and cycled through 7, 21, 35, and 49 $\mathrm{mT\,m^{-1}}$ in successive transients. In (b), the x, y ^{1}H purge pulses immediately after the acquisition are applied for 8 and 5 ms respectively, with a 10 kHz field. The ^{13}C pulses are centered at 67 ppm. The first 180° ^{13}C pulse is a composite $90°_x180°_y90°_x$ pulse. The GARP decoupling is preceded by high-power ^{15}N and ^{13}C pulse pairs as described by Bax et al.[33] The delays τ_a and τ_b were both set to 1.7 ms. Quadrature in t_1 and t_2 is achieved via States–TPPI[13] of ϕ_1 and ϕ_2, respectively. The diagram at the bottom of the figure illustrates the adjustment of timing delays in order to obtain a 180° first-order phase correction in F_2 for both ^{15}N- and ^{13}C-modulated data. The first ^{13}C pulse, of duration pwc, commences at $\delta_1 = [(\pi - 2)/\pi](\mathrm{pwn} - \mathrm{pwc})$ after the start of the ^{15}N ϕ_2 pulse of duration pwn, while the ^{13}C pulse immediately after the t_2 evolution period begins $\delta_2 = (2/\pi)(\mathrm{pwn} - \mathrm{pwc})$ after the start of the corresponding ^{15}N pulse (pwc < pwn). By setting the initial t_2 value, $t_2(0) = (2\mathrm{SW}_2)^{-1} - [(4/\pi)\mathrm{pwn} + 2\mathrm{pw}]$, where SW_2 is the spectral width in the ^{13}C and ^{15}N dimensions and pw is the ^{1}H 90° pulse width, a 180° first-order phase correction in F_2 is obtained. The following phase cycle is employed: $\phi_1 = 4(x),4(-x)$; $\phi_2 = 8(x),8(-x)$; $\phi_3 = (x,y,-x,-y)$; $\phi_4 = 4(x),4(-x)$; rec. = $(x,-y,-x,y,-x,y,x,-y,-x,y,x,-y,x,-y,-x,y)$. The durations and strengths of the gradients are g_1 = (3 ms, 150 $\mathrm{mT\,m^{-1}}$), g_2 = (1 ms, 200 $\mathrm{mT\,m^{-1}}$), $g_3 = g_4$ = (1 ms, 80 $\mathrm{mT\,m^{-1}}$), g_5 = (4 ms, 300 $\mathrm{mT\,m^{-1}}$), g_6 = (3 ms, −180 $\mathrm{mT\,m^{-1}}$), and $g_7 = g_8$ = (1 ms, 80 $\mathrm{mT\,m^{-1}}$). A delay of at least 50 μs between the application of a gradient pulse and the subsequent application of an rf pulse is employed. All gradient pulses are rectangular in shape. (Adapted from (a) Vuister et al.[30] and (b) Pascal et al.[32])

For References see p. 4743

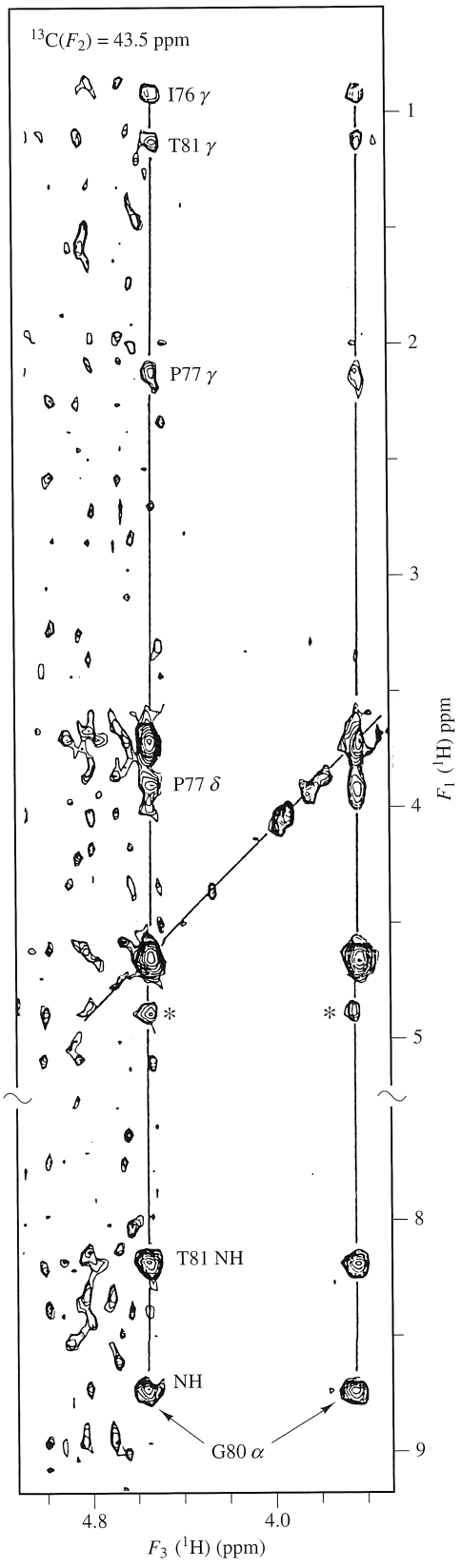

sion. A detailed description of the utility of each gradient is found elsewhere.[32] Gradients g_5 and g_6 are particularly important for water suppression, since, during the time of their application, the magnetization of interest is of the form $\hat{I}_z\hat{X}_z$, where $\hat{I}_z$ and $\hat{X}_z$ are the z components of ^{1}H and ^{15}N or ^{13}C magnetizations, respectively, while water magnetization is present in the transverse plane and hence is dephased by the combined action of the gradient pair (g_5, g_6). For this reason, an HSQC-type transfer of magnetization from ^{1}H to X must be employed rather than an HMQC transfer.[34,35] Figure 5 illustrates the quality of water suppression obtained with the present sequence with the ^{15}N pulses set to zero (i.e., ^{13}C NOESY–HSQC) for a 1.5 mM sample of the cellulose binding domain CBD. The noise from the residual water obscures a region of approximately ±0.2 ppm around the water line (4.8 ppm) in F_3.

The basic flow of magnetization transfer in this experiment can be described by the following two independent pathways:

$$^1\mathrm{H}(t_1) \xrightarrow{\mathrm{NOE}} \mathrm{NH} \xrightarrow{J(\mathrm{N,H})} {}^{15}\mathrm{N}(t_2) \xrightarrow{J(\mathrm{N,H})} \mathrm{NH}(t_3) \tag{9}$$

$$^1\mathrm{H}(t_1) \xrightarrow{\mathrm{NOE}} \mathrm{CH} \xrightarrow{J(\mathrm{C,H})} {}^{13}\mathrm{C}(t_2) \xrightarrow{J(\mathrm{C,H})} \mathrm{CH}(t_3) \tag{10}$$

with chemical shifts recorded during t_1, t_2, and t_3. Note that each (F_1, F_3) slice of the data set is labeled with either the ^{15}N or ^{13}C chemical shift of the heteroatom to which the destination proton is attached. For proteins, ^{13}C- and ^{15}N-bound protons generally have quite distinct chemical shifts, and therefore, with the possible exception of a few backbone or side-chain amide and aromatic protons, the extra information in these spectra relative to single ^{15}N- or ^{13}C-edited data sets does not create ambiguities in interpretation.

A particularly important feature of the CN NOESY–HSQC data set is that, for each NOE cross peak between a carbon-bound proton and a nitrogen-bound proton at position (CH,N,NH), it is possible to find a symmetry-related cross peak at (NH,C,CH). The experiment also provides NOEs between exclusively carbon-bound or nitrogen-bound protons. Figure 6 shows a number of slices from a 150 ms CN NOESY–HSQC data set obtained on a 1.5 mM sample of the C-terminal SH2 domain from phospholipase-Cγ1 complexed with a 12-residue phosphotyrosine-containing peptide.

Figure 5 Section of an (F_1, F_3) slice from the 3D gradient ^{13}C NOESY–HSQC spectrum recorded at 500 MHz on a 1.5 mM sample of ^{15}N-,^{13}C-labeled CBD, pH 7.0, 90% H_2O/10% D_2O at 30 °C, displaying a region close to the water resonance. The mixing time was 150 ms and the data set was acquired as a 128 × 32 × 416 complex matrix (t_1, t_2, t_3), in about 90 h. The data were processed to give absorptive spectra consisting of 256 × 64 × 1024 points in each of (F_1, F_2, F_3). Residual water not eliminated by the gradients was removed using a postacquisition time domain deconvolution procedure.[35] Cross peaks due to either NOEs to water or exchange with labile groups are indicated with asterisks. Interresidue NOEs are labeled with the residue name. (Adapted from Muhandiram et al.[35])

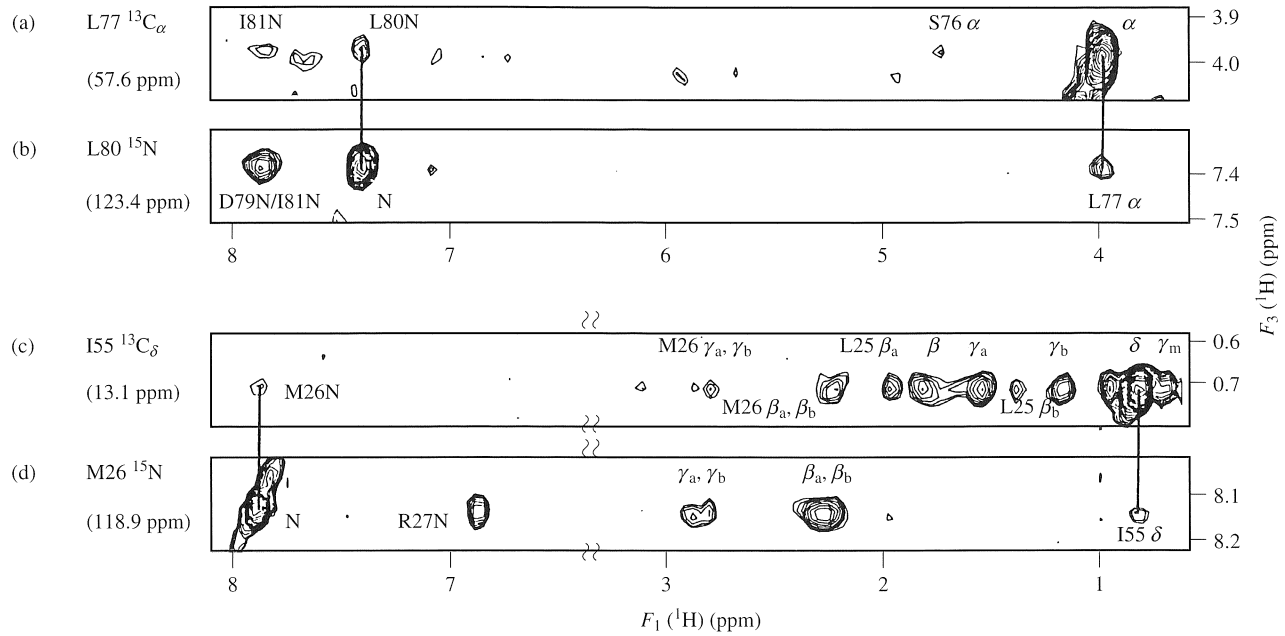

Figure 6 Slices from a CN NOESY-HSQC data set recorded at 500 MHz on a 1.5 mM sample of the protein–peptide complex PLCγ1 SH2-pY1021, showing pairs of 'symmetry-related' cross peaks for NOEs between L80NH and L77C$_\alpha$H (a, b) and M26NH and 155C$_\delta$H (c, d). The cross peaks are observed on planes with the appropriate F_2 chemical shift being either that of ^{15}N or ^{13}C, depending on whether the destination proton is an amide or aliphatic proton. The cross peak of interest from each slice is connected to the diagonal on the corresponding slice by a vertical line. Peaks are labeled with the atom name, and interresidue NOEs are additionally labeled with the residue name. The NOE mixing time was 150 ms, and the data set was acquired as a 128 × 32 × 416 complex matrix (t_1, t_2, t_3), in about 90 h. The data set was processed to give absorptive spectra consisting of 256 × 128 × 1024 points in each of (F_1, F_2, F_3). In order to optimize the resolution of the ^{15}N lines, linear prediction was employed in t_2. The intensity of the residual water signal was minimized through the time domain deconvolution procedure discussed by Muhandiram et al.[35] (Reproduced by permission of Academic Press from S. M. Pascal, D. R. Muhandiram, T. Yamazaki, J. D. Forman-Kay, and L. E. Kay, *J. Magn. Reson., Ser B*, 1994, **103**, 197)

4 SENSITIVITY-ENHANCED VERSIONS OF 3D HETERONUCLEAR-EDITED NOESY EXPERIMENTS

In the past several years, a family of elegant pulse schemes has been developed by Cavanagh, Palmer, and Rance that offers significant improvements in sensitivity for certain classes of experiments.[36,37] In the case of a two-dimensional experiment, for example, sensitivity gains are recognized because both the cosine- and the sine-modulated t_1 components are refocused into observable magnetization prior to detection. In this section, a description of a nongradient, sensitivity-enhanced ^{15}N-edited NOESY–HMQC experiment[37] is presented, followed by a discussion of a sensitivity-enhanced ^{15}N-edited NOESY–HSQC gradient experiment.[38] In the latter experiment, saturation of water is minimized as well by employing selective pulses on water to restore magnetization to the $+z$ axis prior to detection.

4.1 Sensitivity-Enhanced 3D ^{15}N-Edited NOESY–HMQC

Figure 7(a) illustrates the pulse scheme used to record ^{15}N-edited NOESY–HMQC spectra with increased sensitivity.[37] Although the sequence is slightly more complicated than the unenhanced version illustrated in Figure 2(b), the flow of magnetization throughout the experiment is easily understood with the use of the product operator formalism.[18] Immediately prior to detection, the magnetization that originates on spin a and is transferred to spin b is described by

$$\hat{\rho}(\phi_2 = x) = A[-\hat{I}_{bx}\cos(\omega_N t_2) - \delta_{1,M}\hat{I}_{by}\sin(\omega_N t_2)]\cos(\omega_a t_1) \quad (11)$$

$$\hat{\rho}(\phi_2 = -x) = A[\hat{I}_{bx}\cos(\omega_N t_2) - \delta_{1,M}\hat{I}_{by}\sin(\omega_N t_2)]\cos(\omega_a t_1) \quad (12)$$

where $\hat{\rho}$ is the density operator, M is the number of protons (spins I) attached to the heterospin (spin N), A is a factor that depends, among other things, on the efficiency of transfer of I-spin magnetization from spin a to spin b, and $\delta_{1,M} = 1$ if $M = 1$ and zero otherwise. Note that separate data sets are recorded for $\phi_2 = x$ and $\phi_2 = -x$. Using the present approach, phase-modulated data are generated in the t_2 dimension, as equations (11) and (12) suggest.

In order to generate pure absorptive lineshapes, the data can be recombined by taking the sum and the difference of the data sets obtained for $\phi_2 = \pm x$ for a given value of t_2 to generate a new data set of the form

$$(11) + (12) \quad \hat{\rho} = -\delta_{1,M}2A\hat{I}_{by}\cos(\omega_a t_1)\sin(\omega_N t_2) \quad \text{(SUM)} \quad (13)$$

$$(11) - (12) \quad \hat{\rho} = -2A\hat{I}_{bx}\cos(\omega_a t_1)\cos(\omega_N t_2) \quad \text{(DIFFERENCE)} \quad (14)$$

For References see p. 4743

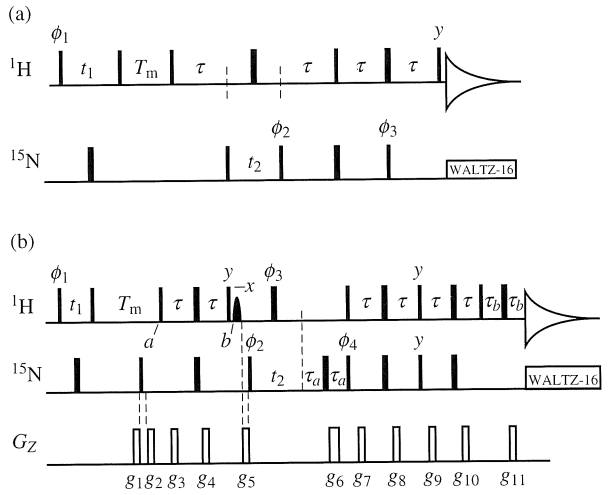

Figure 7 Pulse sequences for (a) sensitivity-enhanced 3D NOESY–HMQC and (b) sensitivity-enhanced gradient 3D NOESY–HSQC experiments. Unless otherwise stated, all parameters are as in Figure 2. In both experiments, quadrature in t_1 is achieved by States–TPPI of ϕ_1. (a) The phase cycle is $\phi_1 = x,-x$; $\phi_2 = 2(x),2(-x)$; $\phi_3 = 2(y),2(-y)$; Rec. $= x,2(-x),x$. The phase of ϕ_2 is inverted after four transients, and the data are stored separately. Quadrature in t_2 is achieved using the method of States.[19] (b) The shaped pulse on ^{1}H is a 'water'-selective 90° pulse. This pulse is either a 2 ms rectangular pulse (125 Hz field) or a 2 ms shaped pulse (270 Hz field at peak height) having the profile of a 90° SEDUCE-1 element.[16] The phase cycle is $\phi_1 = x,-x$; $\phi_2 = 4(x),4(-x)$; $\phi_3 = 2(x),2(-x)$; $\phi_4 = x$; Rec. $= 2(x,-x),2(-x,x)$. For each t_2 increment, the phase ϕ_2 and the receiver phase are inverted. For each t_2 value, two FIDs are recorded and stored separately, with the phase ϕ_4 and the amplitude of the gradient pulse g_{11} inverted for the second FID. The delays τ, τ_a and τ_b are set to 2.4 ms ($<[4J(\mathrm{N,H})]^{-1}$), 1.5 ms and 0.5 ms respectively. The durations and strengths of the gradients are g_1 = (2 ms, 100 mT m^{-1}), g_2 = (0.5 ms, 80 mT m^{-1}), $g_3 = g_4$ = (0.75 ms, 50 mT m^{-1}), g_5 = (2 ms, −150 mT m^{-1}), g_6 = (1.25 ms, 300 mT m^{-1}), $g_7 = g_8$ = (0.5 ms, 80 mT m^{-1}), $g_9 = g_{10}$ = (0.5 ms, 50 mT m^{-1}), and g_{11} = (0.125 ms, 278 mT m^{-1}). The strength of g_{11} is optimized by maximizing the signal. (Adapted from (a) Palmer et al.[37] and (b) Zhang et al.[38])

Note that the SUM signal is proportional to $\hat{I}_y$, while the DIFFERENCE signal is proportional to $\hat{I}_x$. For this reason, a 90° zeroth-order phase correction is applied to either the SUM or the DIFFERENCE data (not both) in the time domain. After these simple time-domain manipulations have been performed, a data set is obtained that contains peaks that are purely absorptive after processing using the States recipe.[19] For the case where $M = 1$ (i.e., an AX ^{15}N,NH heteronuclear spin system) the process of taking the sum and the difference of the signals described by equations (11) and (12) increases the signal intensity by a factor of two relative to signals in spectra recorded using an unenhanced sequence. The noise floor increases by a factor of $\sqrt{2}$ during this process, so that the net increase in signal-to-noise ratio is a factor of $\sqrt{2}$. Of course, this theoretical sensitivity gain does not include potential losses that can occur owing to the increased number of pulses and delays in the sequence relative to the unenhanced version. For protein applications considered to date, appreciable increases in sensitivity have been obtained. Figure 8 compares the F_1 traces from regular and sensitivity-enhanced NOESY–HMQC spectra

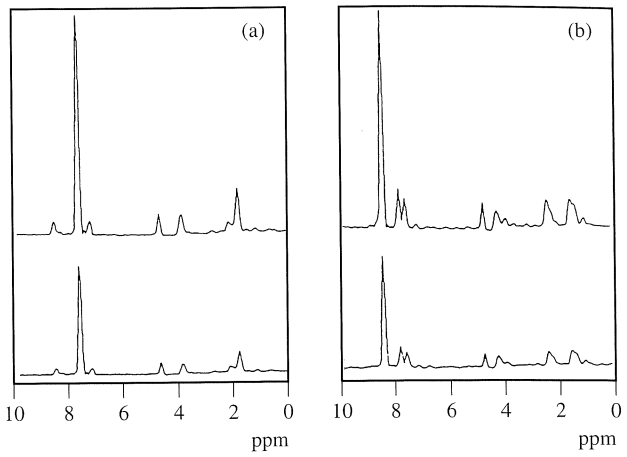

Figure 8 Comparison of conventional (bottom trace) and sensitivity-enhanced NOESY–HMQC (top trace) spectra of the protein calbindin recorded at 500 MHz. Both experiments were acquired in the same overall time as 100 × 32 × 1024 complex data sets with 16 transients per FID. The NOE mixing time was 150 ms. The figure shows F_1 cross sections for (a) Lys12 and (b) Glu35 taken at F_2, F_3 frequencies of the backbone amide ^{15}N and proton resonances, respectively. The increase in the RMS baseplane noise for the enhanced spectrum, compared with the conventional one, agrees with the theoretical value of $\sqrt{2}$. The average S/N improvements between the enhanced and conventional spectra are (a) 1.41 and (b) 1.39. (Reproduced by permission of Academic Press from A. G. Palmer, J. Cavanagh, R. A. Byrd, and M. Rance, *J. Magn. Reson.*, 1992, **96**, 416)

of ^{15}N-labeled calbindin D9k (75 amino acids) in 90% H_2O/10% D_2O, with sensitivity enhancements close to the theoretical maximum of $\sqrt{2}$ realized.

4.2 Sensitivity-Enhanced Gradient 3D NOESY–HSQC

Figure 7(b) illustrates the sensitivity-enhanced 3D ^{15}N-edited NOESY–HSQC sequence with gradients used to suppress artifacts, to aid in the suppression of the intense solvent signal and to select for ^{15}N magnetization during the nitrogen evolution time t_2. In the selection of ^{15}N magnetization using gradients, a sensitivity enhancement approach is taken based on the nongradient sensitivity-enhanced method discussed above.[23] Sensitivity in the experiment is increased further by restoring the water signal to the $+z$ axis prior to detection[25] in order to minimize the saturation of water during the course of the experiment. The detailed mechanism of the experiment is reported elsewhere.[38] It can easily be understood how the water is stored along the $+z$ axis after each transient by noting that for mixing times T_m in excess of about 50 ms, the effect of radiation damping is such that water magnetization is restored to the $+z$ axis at point a in the pulse scheme in a manner independent of the phase ϕ_1 of the first ^{1}H 90° pulse. In order to facilitate radiation damping, ϕ_1 is phase-cycled 45°, 225° as opposed to 0°, 180° (x, $-x$). Immediately after the first ^{1}H $90°_y$ pulse (point b in the sequence), the water magnetization is along the y axis, while the signal of interest is of the form $\hat{I}_z\hat{N}_z$, where $\hat{I}_z$ and $\hat{N}_z$ are the z components of the NH and ^{15}N magnetizations, respectively. The water-selective pulse applied at this point rotates the (on-resonance) water magnetization to the $-z$ axis without perturbing the signal of interest. Application

of the gradient g_5 immediately after the selective pulse ensures that any residual water magnetization in the transverse plane is completely dephased, thereby eliminating radiation damping at this point. It is straightforward to show that the effect of the remaining proton pulses on the water is such that water magnetization resides along the $+z$ axis at the start of the acquisition period t_3.

A product operator description similar to that given above shows that, immediately prior to acquisition, the magnetization associated with an NH proton is given by

$$\hat{\rho}(\phi_4 = \pm x) = A\cos(\omega_a t_1)[\pm\hat{I}_{by}\cos\theta_1 + \hat{I}_{bx}\sin\theta_1] \qquad (15)$$

where $\hat{I}_{bx}$ and $\hat{I}_{by}$ are the x and y components of NH magnetization, and all other symbols defined as above. The value of θ_1 is given by $\theta_1 = \omega_N t_2 + \gamma_N B_1(z)\tau_1 \pm \gamma_H B_2(z)\tau_2$ for $\phi_4 = \pm x$, where ω_N is the ^{15}N Larmor frequency, γ_i is the gyromagnetic ratio of spin i, and τ_i ($i = 1, 2$) is the duration of the z gradient pulse generating a magnetic field of magnitude B_i at position z in the sample. Assuming that

1. the gradients used to select for ^{15}N magnetization (g_6, g_{11}) are sufficiently strong that they cause complete dephasing of magnetization, and
2. for $\phi_4 = \pm x$, the gradients are adjusted so that $\gamma_N B_1(z)\tau_1 = \mp\gamma_H B_2(z)\tau_2$,

Equation (15) reduces to

$$\hat{\rho}(\phi_4 = \pm x) = A\cos(\omega_a t_1)[\pm\hat{I}_{by}\cos(\omega_N t_2) + \hat{I}_{bx}\sin(\omega_N t_2)] \qquad (16)$$

For each value of t_2, data sets are recorded with $\phi_4 = x$, $\gamma_N B_1(z)\tau_1 = -\gamma_H B_2(z)\tau_2$, and $\phi_4 = -x$, $\gamma_N B_1(z)\tau_1 = \gamma_H B_2(z)\tau_2$, and stored in separate memory locations. The data are subsequently manipulated in the time domain, as described in connection with the enhanced NOESY–HMQC experiment above, to yield a purely absorptive spectrum after Fourier transformation. Enhancements in signal-to-noise ratio by a factor of as much as $\sqrt{2}$ relative to unenhanced experiments can be obtained using this approach.

5 CONCLUDING REMARKS

The development of heteronuclear, multidimensional, multinuclear MR spectroscopy has facilitated large numbers of structural studies of macromolecules, and has significantly increased the size of molecules that can be studied. The heteronuclear-edited NOESY experiment provides the crucial distance information necessary for these structure determinations. Presently, the interpretation of NOESY data sets is the time-consuming step in the structure determination process. Current efforts are focusing on ways of providing a more automated approach to the assignment of NOE cross peaks and the calculation of structures.

6 RELATED ARTICLES

Biological Macromolecules: Structure Determination in Solution; Field Gradients & Their Application; Heteronuclear Shift Correlation Spectroscopy; Multidimensional Spectroscopy: Concepts; NOESY; Nuclear Overhauser Effect; Structures of Larger Proteins, Protein–Ligand, & Protein–DNA Complexes by Multi-Dimensional Heteronuclear NMR; Three- & Four-Dimensional Heteronuclear Magnetic Resonance.

7 REFERENCES

1. J. Jeener, B. H. Meier, P. Bachmann, and R. R. Ernst, *J. Chem. Phys.*, 1979, **71**, 4546.
2. S. W. Fesik and E. R. P. Zuiderweg, *Quart. Rev. Biophys.*, 1990, **23**, 97.
3. A. Bax and S. Grzesiek, *Acc. Chem. Res.*, 1993, **26**, 131.
4. L. P. McIntosh and F. W. Dahlquist, *Quart. Rev. Biophys.*, 1990, **23**, 1.
5. G. M. Clore and A. M. Gronenborn, in 'Progress in Nuclear Magnetic Resonance Spectroscopy', eds. J. W. Emsley, J. Feeney, and L. H. Sutcliffe, Pergamon Press, Oxford, 1991, Vol. 23, p. 43.
6. G. Wagner, *J. Biomol. NMR*, 1993, **3**, 375.
7. E. P. Nikonowicz and A. Pardi, *Nature (London)*, 1992, **355**, 184.
8. P. de Waard, B. R. Leeflang, J. F. G. Vliegenthart, R. Boelens, G. W. Vuister, and R. Kaptein, *J. Biomol. NMR*, 1992, **2**, 211.
9. A. Bax, R. H. Griffey, and B. L. Hawkins, *J. Magn. Reson.*, 1983, **55**, 301.
10. G. Bodenhausen and D. J. Ruben, *Chem. Phys. Lett.*, 1980, **69**, 185.
11. S. W. Fesik and E. R. P. Zuiderweg, *J. Magn. Reson.*, 1988, **78**, 588.
12. D. Marion, L. E. Kay, S. W. Sparks, D. A. Torchia, and A. Bax, *J. Am. Chem. Soc.*, 1989, **111**, 1515.
13. D. Marion, M. Ikura, R. Tschudin, and A. Bax, *J. Magn. Reson.*, 1989, **85**, 393.
14. A. J. Shaka, J. Keeler, T. Frenkiel, and R. Freeman, *J. Magn. Reson.*, 1983, **52**, 335.
15. A. J. Shaka, P. B. Barker, and R. Freeman, *J. Magn. Reson.*, 1985, **64**, 547.
16. M. A. McCoy and L. Mueller, *J. Am. Chem. Soc.*, 1992, **114**, 2108.
17. M. Ikura, L. E. Kay, R. Tschudin, and A. Bax, *J. Magn. Reson.*, 1990, **86**, 204.
18. O. W. Sørensen, G. W. Eich, M. H. Levitt, G. Bodenhausen, and R. R. Ernst, in 'Progress in Nuclear Magnetic Resonance Spectroscopy', eds. J. W. Emsley, J. Feeney, and L. H. Sutcliffe, Pergamon Press, Oxford, 1983, Vol. 16, p. 163.
19. D. J. States, R. A. Haberkorn, and D. J. Ruben, *J. Magn. Reson.*, 1982, **48**, 286.
20. J. H. Noggle and R. E. Schirmer, 'The Nuclear Overhauser Effect', Academic Press, New York, 1971.
21. L. E. Kay, D. Marion, and A. Bax, *J. Magn. Reson.*, 1989, **84**, 72.
22. G. A. Morris and R. Freeman, *J. Magn. Reson.*, 1978, **29**, 433.
23. L. E. Kay, P. Keifer, and T. Saarinen, *J. Am. Chem. Soc.*, 1992, **114**, 10 663.
24. Y. C. Li and G. T. Montelione, *J. Magn. Reson., Ser. B*, 1993, **101**, 315.
25. S. Grzesiek and A. Bax, *J. Am. Chem. Soc.*, 1993, **115**, 12 593.
26. A. Bax, M. Ikura, L. E. Kay, and G. Zhu, *J. Magn. Reson.*, 1991, **91**, 174.
27. D. Marion and A. Bax, *J. Magn. Reson.*, 1989, **83**, 205.
28. B. K. John, D. Plant, P. Webb, and R. E. Hurd, *J. Magn. Reson.*, 1992, **98**, 200.
29. A. Bax and S. S. Pochapsky, *J. Magn. Reson.*, 1992, **99**, 638.
30. G. W. Vuister, R. Boelens, R. Kaptein, M. Burgering, and P. C. M. van Zijl, *J. Biomol. NMR*, 1992, **2**, 301.
31. R. E. Hurd and B. K. John, *J. Magn. Reson.*, 1991, **91**, 648.
32. S. M. Pascal, D. R. Muhandiram, T. Yamazaki, J. D. Forman-Kay, and L. E. Kay, *J. Magn. Reson., Ser. B*, 1994, **103**, 197.

33. A. Bax, G. M. Clore, P. C. Driscoll, A. M. Gronenborn, M. Ikura, and L. E. Kay, *J. Magn. Reson.*, 1990, **87**, 620.
34. A. Majumdar and E. R. P. Zuiderweg, *J. Magn. Reson., Ser. B*, 1993, **102**, 242.
35. D. R. Muhandiram, N. A. Farrow, G. Y. Xu, S. H. Smallcombe, and L. E. Kay, *J. Magn. Reson., Ser. B*, 1993, **102**, 317.
36. A. G. Palmer, J. Cavanagh, P. E. Wright, and M. Rance, *J. Magn. Reson.*, 1991, **93**, 151.
37. A. G. Palmer, J. Cavanagh, R. A. Byrd, and M. Rance, *J. Magn. Reson.*, 1992, **96**, 416.
38. O. Zhang, L. E. Kay, J. P. Olivier, and J. D. Forman-Kay, *J. Biomol. NMR*, 1994, **4**, 845.

Biographical Sketches

Lewis E. Kay. *b* 1961. B.Sc., 1983, University of Alberta, Canada; Ph.D., 1987, Yale University, USA. Postdoctoral work at the National Institutes of Health, USA (with Ad Bax), 1987–92. Professor, Departments of Medical Genetics, Biochemistry and Chemistry at the University of Toronto, 1992–present. Current research interests: development of multinuclear, multidimensional NMR methods for the study of structure and dynamics of proteins.

Ranjith Muhandiram. *b* 1956. B.Sc., 1979, University of Colombo, Sri Lanka; Ph.D., 1987, University of Alberta, Canada (supervisor R. E. D. McClung). Postdoctoral work at the University of Alberta (with R. E. D. McClung), 1987–89. Research associate at the National Research Council, Canada, 1989–92. Research associate with Professor Kay, 1992–present.

Three- & Four-Dimensional Heteronuclear Magnetic Resonance

G. Marius Clore & Angela M. Gronenborn
National Institutes of Health, Bethesda, MD, USA

1 WHY ARE THREE- (3D) AND FOUR-DIMENSIONAL (4D) EXPERIMENTS REQUIRED?

The principal source of geometric information used to solve 3D structures of macromolecules by NMR resides in short (<5 Å), approximate, interproton distance restraints derived from nuclear Overhauser enhancement (NOE) measurements.[1–7] In order to extract this information it is essential first to completely assign the ^{1}H spectrum of the macromolecule in question and then to assign as many structurally useful NOE interactions as possible. The larger the number of NOE restraints, the higher the precision and accuracy of the resulting structures.[7–9] Indeed, with current state-of-the-art methodology it is now possible to obtain NMR structures of proteins at a precision and accuracy comparable to 2 Å resolution crystal structures.[8–12]

For proteins of 100 residues or less, conventional homonuclear two-dimensional (2D) NMR methods can be applied with a considerable degree of success.[1–7,13,14] As the number of residues and molecular weight increases beyond 100 kDa and 12 kDa, respectively, two main obstacles present themselves, which has made it necessary to extend the 2D NMR techniques to higher dimensions and to develop new approaches. First, the increased spectral complexity arising from the presence of a larger number of protons results in extensive chemical shift overlap and degeneracy, rendering the 2D spectra uninterpretable. Second, the rotational correlation time increases with molecular weight resulting in large ^{1}H linewidths and a concomitant severe decrease in the sensitivity of correlation experiments based on intrinsically small three-bond ^{1}H–^{1}H couplings. These obstacles can be overcome by increasing the dimensionality of the spectra to resolve problems associated with spectral overlap and by simultaneously making use of heteronuclear couplings that are larger than the linewidths to circumvent limitations in sensitivity.[8,9] This approach necessi-